

 Open access • Posted Content • DOI:10.1101/2020.06.25.170399

Structure and allosteric regulation of human IDH3 holoenzyme — [Source link](#)

[Jianping Ding](#), [Peng kai Sun](#), [Yan Liu](#), [Tengfei Ma](#)

Institutions: [Chinese Academy of Sciences](#), [ShanghaiTech University](#)

Published on: 25 Jun 2020 - [bioRxiv](#) (Cold Spring Harbor Laboratory)

Topics: [Allosteric regulation](#)

Related papers:

- [Structure and allosteric regulation of human NAD-dependent isocitrate dehydrogenase.](#)
- [Dynamic Coupling and Allosteric Networks in the \$\alpha\$ Subunit of Heterotrimeric G Proteins.](#)
- [Allosteric regulation of DegS protease subunits through a shared energy landscape](#)
- [Allosteric Response of DNA Recognition Helices of Catabolite Activator Protein to cAMP and DNA Binding](#)
- [Structural basis of CK2 regulation by autoinhibitory oligomerization](#)

Share this paper:    

View more about this paper here: <https://typeset.io/papers/structure-and-allosteric-regulation-of-human-idh3-holoenzyme-lr7kx3cauv>

1 **Structure and allosteric regulation of human IDH3 holoenzyme**

2 **Pengkai Sun¹, Yan Liu², Tengfei Ma¹, and Jianping Ding^{1,2,3,*}**

3 ¹ State Key Laboratory of Molecular Biology, Shanghai Institute of Biochemistry and Cell
4 Biology, Center for Excellence in Molecular Cell Science, University of Chinese Academy of
5 Sciences, Chinese Academy of Sciences, 320 Yueyang Road, Shanghai 200031, China

6 ² School of Life Science and Technology, ShanghaiTech University, 393 Huaxia Zhong Road,
7 Shanghai 201210, China

8 ³ School of Life Science, Hangzhou Institute for Advanced Study, University of Chinese
9 Academy of Sciences, 1 Xiangshan Road, Hangzhou 310024, China

10

11 * Correspondence: Jianping Ding (Phone: +86-21-54921619, E-mail: jpding@sibcb.ac.cn).

12 **Running title:** Crystal structure of human NAD-IDH

13 **Keywords:** Isocitrate dehydrogenase, IDH, NAD-IDH, assembly, allosteric regulation.

14

15 **Abstract** Human NAD-dependent isocitrate dehydrogenase or IDH3 catalyzes the
16 decarboxylation of isocitrate into α -ketoglutarate in the TCA cycle. We here report the
17 structure of the IDH3 holoenzyme, in which the $\alpha\beta$ and $\alpha\gamma$ heterodimers assemble the $\alpha_2\beta\gamma$
18 heterotetramer via their clasp domains, and two $\alpha_2\beta\gamma$ heterotetramers assemble the $(\alpha_2\beta\gamma)_2$
19 heterooctamer via the β and γ subunits. The functional roles of the key residues involved in
20 the assembly and allosteric regulation are validated by mutagenesis and kinetic studies. The
21 allosteric site plays an important role but the pseudo allosteric site plays no role in the
22 allosteric activation; the activation signal from the allosteric site is transmitted to the active
23 sites of both heterodimers via the clasp domains; and the N-terminus of the γ subunit plays a
24 critical role in the formation and function of the holoenzyme. These findings reveal the
25 molecular mechanism of the assembly and allosteric regulation of human IDH3 holoenzyme.
26

27 **Introduction**

28 In all aerobic organisms, the cells use the tricarboxylic acid (TCA) cycle (also called citric
29 acid cycle or Krebs cycle) to generate ATP through oxidation of acetyl-CoA derived from
30 carbohydrates, fats, and proteins. In addition, the TCA cycle also provides intermediates for
31 de novo synthesis of proteins, lipids and nucleic acids (Pavlova and Thompson, 2016).
32 Among a series of biochemical reactions in the TCA cycle, isocitrate dehydrogenases (IDHs)
33 catalyze oxidative decarboxylation of isocitrate (ICT) into α -ketoglutarate (α -KG) using
34 NAD or NADP as coenzyme. Most prokaryotes contain only NADP-dependent IDHs
35 (NADP-IDHs) in the cytosol, which exert the catalytic function. Eukaryotes contain both
36 NADP-IDHs and NAD-dependent IDHs (NAD-IDHs). In human and other mammalian cells,
37 there are two NADP-IDHs and one NAD-IDH: the two NADP-IDHs are located to the
38 cytosol and the mitochondria and are called IDH1 and IDH2, respectively, and the NAD-IDH
39 is located to the mitochondria and is called IDH3. It is well established that IDH3 exerts the
40 catalytic function in the TCA cycle (Al-Khallaf, 2017). Both IDH1 and IDH2 play important
41 roles in cellular defense against oxidative damage, removal of reactive oxygen species, and
42 synthesis of fat and cholesterol (Jo et al., 2001; Kim and Park, 2003; Koh et al., 2004; Lee et
43 al., 2002). Aberrant functions of all three enzymes have been implicated in the pathogenesis
44 of numerous metabolic diseases (Hartong et al., 2008; Kiefmann et al., 2017; Yoshimi et al.,
45 2016) and malignant tumors (Dang et al., 2009; May et al., 2019; Waitkus et al., 2016; Yan et
46 al., 2009; Zhang et al., 2015).

47 Both prokaryotic and eukaryotic NADP-IDHs exist and function as homodimers in
48 which both subunits have catalytic activity (Hurley et al., 1991; Xu et al., 2004). These
49 enzymes share a conserved catalytic mechanism, but have different regulatory mechanisms.
50 The activity of *Escherichia coli* NADP-IDH is regulated through reversible phosphorylation
51 and dephosphorylation of a strictly conserved Ser residue at the active site by the dual
52 functional kinase/phosphatase AceK, and other bacterial NADP-IDHs might share a similar
53 regulatory mechanism (Zheng and Jia, 2010; Zheng et al., 2012). The activity of human IDH1
54 is regulated through substrate-binding induced conformational change of a key structure
55 element at the active site, and other mammalian NADP-IDHs might utilize a similar
56 regulatory mechanism (Xu et al., 2004; Yang et al., 2010).

57 Compared to NADP-IDHs, NAD-IDHs are composed of different types of subunits with
58 distinct functions and employ more sophisticated regulatory mechanisms. *Saccharomyces*
59 *cerevisiae* NAD-IDH is composed of a regulatory subunit IDH1 and a catalytic subunit IDH2
60 which form the IDH1/IDH2 heterodimer as the basic functional unit, and the heterodimer is
61 assembled into a heterotetramer and further into a heterooctamer (Lin et al., 2011; Lin and
62 McAlister-Henn, 2003; Taylor et al., 2008). IDH2 contains the active site and IDH1 contains

63 the allosteric site, and the binding of activators citrate (CIT) and AMP to the allosteric site can
64 cause conformational changes of the active site through the heterodimer interface, leading to
65 the activation of the enzyme. The composition and regulation of human and other mammalian
66 NAD-IDHs are even more complex than those of yeast NAD-IDH. Human NAD-IDH or
67 IDH3 are composed of three types of subunits in the ratio of $2\alpha:1\beta:1\gamma$ (Nichols et al., 1993;
68 Nichols et al., 1995). The α and β subunits form a heterodimer ($\alpha\beta$) and the α and γ subunits
69 form another heterodimer ($\alpha\gamma$), and the two heterodimers are assembled into the $\alpha_2\beta\gamma$
70 heterotetramer and further into the $(\alpha_2\beta\gamma)_2$ heterooctamer (also called holoenzyme) (Ehrlich
71 and Colman, 1983; Ehrlich et al., 1981).

72 Early biochemical studies of mammalian NAD-IDHs showed that the α subunit is the
73 catalytic subunit, and the β and γ subunits are the regulatory subunits (Cohen and Colman,
74 1972; Ehrlich and Colman, 1981); and the activity of the holoenzyme is positively regulated
75 by CIT and ADP but negatively regulated by ATP and NADH (Gabriel and Plaut, 1984a;
76 Gabriel et al., 1985; Gabriel and Plaut, 1984b). Our biochemical studies of human IDH3
77 confirmed some results from the previous studies but also revealed some new findings. We
78 found that in the IDH3 holoenzyme, the α subunits of both $\alpha\beta$ and $\alpha\gamma$ heterodimers have
79 catalytic activity; however, only the γ subunit plays a regulatory role via an allosteric
80 regulatory mechanism, while the β subunit plays no regulatory role but is required for the
81 function of the holoenzyme (Ma et al., 2017b). The holoenzyme and the $\alpha\gamma$ heterodimer are
82 positively regulated by CIT and ADP, and negatively regulated by NADH. In addition, these
83 enzymes can be activated by low concentrations of ATP, but inhibited by high concentrations
84 of ATP. In contrast, the $\alpha\beta$ heterodimer cannot be activated by CIT and ADP, and is inhibited
85 by both NADH and ATP. Our detailed structural and biochemical studies of the $\alpha\gamma$ and $\alpha\beta$
86 heterodimers revealed the underlying molecular mechanisms (Liu et al., 2018; Ma et al.,
87 2017a; Sun et al., 2020; Sun et al., 2019). Nevertheless, so far the structure, assembly and
88 regulatory mechanism of human IDH3 holoenzyme are still unknown. Thus, how the $\alpha\beta$ and
89 $\alpha\gamma$ heterodimers are assembled into the $\alpha_2\beta\gamma$ heterotetramer and further into the $(\alpha_2\beta\gamma)_2$
90 heterooctamer is unclear. How the allosteric site in the γ subunit regulates both α subunits in
91 the $\alpha_2\beta\gamma$ heterotetramer is also unclear. In addition, whether the regulatory mechanisms of the
92 $\alpha\beta$ and $\alpha\gamma$ heterodimers are applicable to the holoenzyme remains elusive.

93 In this work, we determined the crystal structure of human IDH3 holoenzyme in apo
94 form. In the holoenzyme, the $\alpha\beta$ and $\alpha\gamma$ heterodimers assemble the $\alpha_2\beta\gamma$ heterotetramer via
95 their clasp domains, and two $\alpha_2\beta\gamma$ heterotetramers assemble the $(\alpha_2\beta\gamma)_2$ heterooctamer
96 through the N-terminus of the γ subunit of one heterotetramer inserting into the back cleft of
97 the β subunit of the other heterotetramer. We further performed mutagenesis and kinetic

98 studies to validate the functional roles of the key residues at the allosteric site, the pseudo
99 allosteric site, the heterodimer interface, and the heterodimer-heterodimer interface, as well as
100 the N-terminus of the γ subunit. Our structural and biochemical data together reveal the
101 molecular mechanism for the assembly and allosteric regulation of human IDH3 holoenzyme.
102

103 **Results**

104 *Preparation and biochemical analysis of human IDH3 holoenzyme*

105 The wild-type human IDH3 holoenzyme was prepared as described previously (Ma et al.,
106 2017b). Crystallization of the wild-type IDH3 holoenzyme yielded crystals at various
107 conditions; however, these crystals diffracted X-rays to low resolution (about 10 Å),
108 prohibiting us from determining the crystal structure. Our previous biochemical and structural
109 studies showed that substitution of the C-terminal region of the β subunit (residues 341-349)
110 with that of the α subunit (residues 330-338) produced a stable $\alpha\beta$ mutant which exhibits
111 similar enzymatic properties as the wild-type enzyme, and this $\alpha\beta$ mutant yielded high quality
112 crystals which allowed us to solve the structure of the $\alpha\beta$ heterodimer (Sun et al., 2019). Thus,
113 we prepared a mutant IDH3 holoenzyme containing the β mutant, which led to successful
114 structure determination of the IDH3 holoenzyme.

115 Like the wild-type holoenzyme, the β mutant holoenzyme exists as a heterooctamer in
116 solution with high purity and homogeneity as shown by SDS-PAGE and size exclusion
117 chromatography (SEC) analyses (**Fig. S1**). The β mutant holoenzyme exhibits almost
118 identical enzymatic properties as the wild-type holoenzyme, indicating that the substitution of
119 the C-terminal region of the β subunit has no effects on the biochemical and enzymatic
120 properties of the holoenzyme (**Fig. S2 and Table S1**). Therefore, we will not distinguish the
121 wild-type and the β mutant holoenzyme hereafter.
122

123 *Structure of human IDH3 holoenzyme*

124 The structure of human IDH3 holoenzyme was solved at 3.47 Å resolution (**Table 1**). The
125 crystals of the IDH3 holoenzyme belong to space group $I4_122$ with each asymmetric unit
126 containing one $\alpha_2\beta\gamma$ heterotetramer. The four polypeptide chains of the heterotetramer are
127 largely well defined with good electron density except for a few N-terminal and/or C-terminal
128 residues, and the α , β , and γ subunits can be distinguished unambiguously based on the
129 differences of numerous residues with large side chains (**Fig. S3**). There are no ligands bound
130 at the active sites, the allosteric site, and the pseudo allosteric site; thus, this structure
131 represents the structure of the IDH3 holoenzyme in apo form. It is noteworthy that the
132 C-terminal region of the β subunit is located on the structure surface and is involved in the
133 crystal packing, which explains why the crystals of the β mutant IDH3 holoenzyme diffracted

134 X-rays better than the crystals of the wild-type IDH3 holoenzyme.

135

136 **Table 1. Statistics of X-ray diffraction data and structure refinement.**

137

Structure	IDH3 Holoenzyme
Diffraction data	
Wavelength (Å)	0.9792
Space group	$I4_122$
Cell parameters	
a, b, c (Å)	204.57, 204.57, 237.88
Resolution (Å)	50.0-3.47 (3.59-3.47)
Observed reflections	585,722
Unique reflections ($I/\sigma(I) > 0$)	32,854
Average redundancy	17.8 (17.8)
Average $I/\sigma(I)$	35.1 (1.7)
Completeness (%)	100.0 (100.0)
R_{merge} (%)	10.1 (187.5)
CC $\frac{1}{2}$ (%)	99.5 (67.6)
Refinement and structure model	
No. of reflections ($F_o > 0\sigma(F_o)$)	30,525
Working set	28,955
Test set	1,570
$R_{\text{work}}/R_{\text{free}}$ factor	0.21/0.25
Total atoms	9,851
Wilson B factor (Å ²)	51.8
Average B factor (Å ²)	56.1
RMS deviations	
Bond lengths (Å)	0.012
Bond angles (°)	1.4
Ramachandran plot (%)	
Most favored	85.8
Allowed	14.2
Disallowed	0.0

Figure 1.

— α subunit — β subunit — γ subunit — N-terminal of γ subunit

138

139

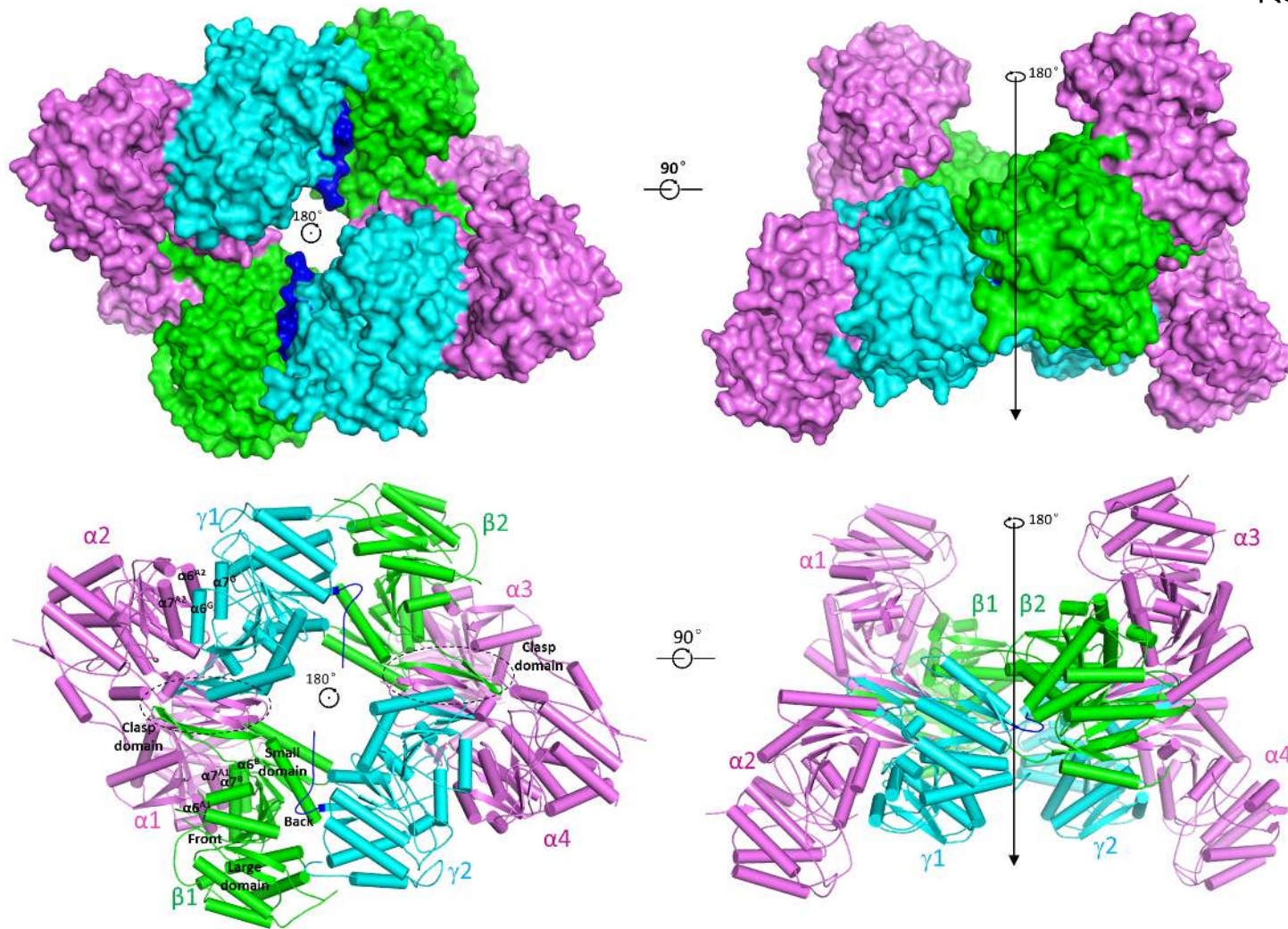


Figure 1. Overall structure of human IDH3 holoenzyme.

(A) Surface and (B) cartoon presentations of human IDH3 holoenzyme in two different orientations. Left: view along the crystallographic 2-fold axis of the IDH3 holoenzyme. Right: view in perpendicular to the crystallographic 2-fold axis of the IDH3 holoenzyme. The α , β and γ subunits are colored in magenta, green and cyan, respectively. The large domain, small domain and clasp domain, and the front and back clefts of the β subunit are indicated. The clasp domains of the $\alpha\beta$ or $\alpha\gamma$ heterodimers are indicated with dashed ovals, and the N-terminal regions of the γ subunits are colored in blue.

161 In the holoenzyme, the $\alpha\beta$ and $\alpha\gamma$ heterodimers assume very similar overall structures as
162 those in the isolated forms (Ma et al., 2017a; Sun et al., 2019) (**Fig. 1**). Both heterodimers
163 have a pseudo two-fold symmetry along the heterodimer interface. The heterodimer interface
164 is mediated by the $\alpha 6$ and $\alpha 7$ helices of the small domains which form a four-helix bundle in
165 a parallel manner, and the $\beta 6$ and $\beta 7$ strands of the clasp domains (the clasp β -strands) which
166 form a four-stranded β -sheet (the clasp β -sheet) in an antiparallel manner. The heterodimer
167 interface buries about 2180 \AA^2 and 2094 \AA^2 solvent accessible surface or 13.7% and 13.5% of
168 the surface area of each subunit in the $\alpha\beta$ and $\alpha\gamma$ heterodimers, respectively, indicating that
169 the heterodimer interface is very tight in both heterodimers.

170 Nevertheless, the $\alpha\beta$ and $\alpha\gamma$ heterodimers in the holoenzyme also exhibit some notable
171 differences from those in the isolated forms. In particular, the $\alpha\beta$ heterodimer assumes an
172 open overall conformation similar to that of the isolated $\alpha\gamma$ heterodimer rather than the
173 compact conformation of the isolated $\alpha\beta$ heterodimer, rendering it suitable for allosteric
174 activation and catalytic reaction (see discussion later). In addition, the N-terminal region
175 (residues 1-14) of the γ subunit is disordered in all of our previously determined $\alpha\gamma$ structures
176 regardless of the presence or absence of ligands; however, a large portion of the N-terminal
177 region (residues 5-14) of the $\alpha\gamma$ heterodimer is well defined in this structure, which plays an
178 important role in the formation and function of the heterooctamer (see discussion later).

179

180 *The heterodimer-heterodimer interface in the $\alpha_2\beta\gamma$ heterotetramer*

181 In the holoenzyme, the $\alpha_2\beta\gamma$ heterotetramer is assembled by the $\alpha\beta$ and $\alpha\gamma$ heterodimers via
182 their clasp domains (**Figs. 1 and 2A**). There is a pseudo two-fold symmetry along the
183 heterodimer-heterodimer interface, which is about 25° off the coplane axis of the $\alpha\beta$ or
184 $\alpha\gamma$ heterodimer. In other words, the coplane axes of the $\alpha\beta$ and $\alpha\gamma$ heterodimers make a 50°
185 angle. Thus, the heterotetramer has a distorted tetrahedron architecture with the two α
186 subunits occupying two vertices on the same side and the β and γ subunits two vertices on the
187 other side (**Fig. 2A**). The heterodimer-heterodimer interface buries about 804 \AA^2 solvent
188 accessible surface or 3.0% of the surface area of each heterodimer. At the interface, the clasp
189 β -sheets of the two heterodimers interact with each other to form a β -barrel in a reciprocal
190 manner such that the clasp β -strands of the β subunit stack antiparallely onto those of the α
191 subunit of the $\alpha\gamma$ heterodimer, and the clasp β -strands of the γ subunit stack antiparallely
192 onto those of the α subunit of the $\alpha\beta$ heterodimer (**Fig. 2A**). The interface consists of
193 twenty-two hydrophobic residues and two Ser residues from the four clasp domains which
194 form extensive hydrophobic interactions (**Fig. 2B**). In addition, there are eight hydrophilic
195 residues which form two layers of hydrogen-bonding interactions to separate the hydrophobic

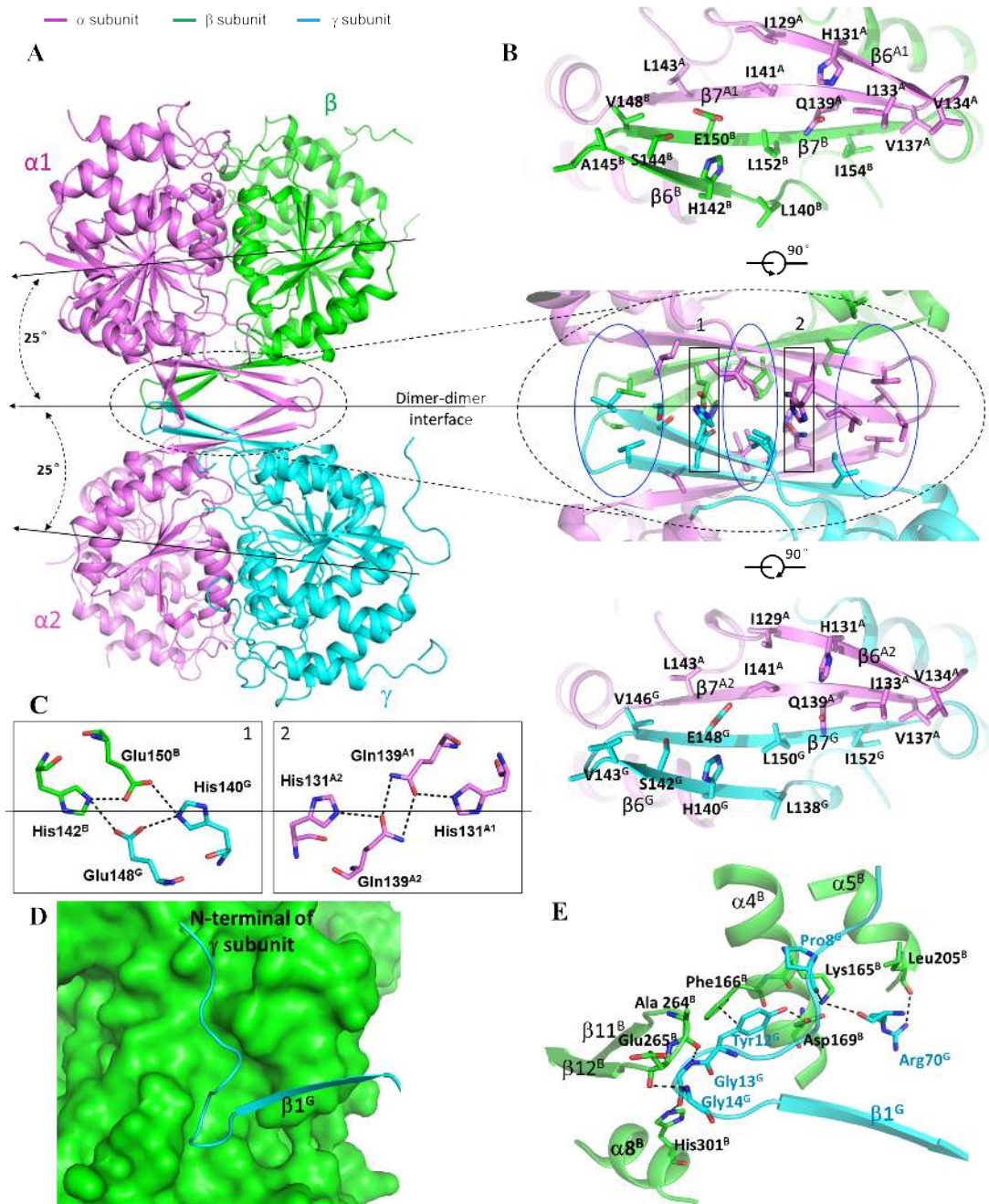
196 interactions (**Figs. 2B and 2C**). Specifically, the side chains of His131^{A1} and Gln139^{A1} of the
197 α subunit in the $\alpha\beta$ heterodimer and His131^{A2} and Gln139^{A2} of the α subunit in the $\alpha\gamma$
198 heterodimer form one network of hydrogen bonds, and the side chains of Gln150^B and
199 His142^B of the β subunit and Gln148^G and His140^G of the γ subunit form another network of
200 hydrogen bonds (residues and structure elements of the α and β subunits of the $\alpha\beta$
201 heterodimer and the α and γ subunits of the $\alpha\gamma$ heterodimer are superscripted by “A1” and
202 “B”, and A2” and “G”, respectively).

203

204 *The heterotetramer-heterotetramer interface in the $(\alpha_2\beta\gamma)_2$ heterooctamer*

205 In the holoenzyme, the $(\alpha_2\beta\gamma)_2$ heterooctamer is assembled by two $\alpha_2\beta\gamma$ heterotetramers
206 related by a crystallographic two-fold symmetry via the β and γ subunits (**Fig. 1**). Thus, the
207 heterooctamer has a distorted tetrahedron architecture, in which the two β and two γ subunits
208 are arranged alternately to form the inner core, and the four α subunits are positioned on the
209 periphery. The heterotetramer-heterotetramer interface buries about 2248 Å² solvent
210 accessible surface or 4.3% of the surface area of the heterotetramer. At the interface, the
211 N-terminal region of the γ subunit of one heterotetramer intrudes into a shallow cleft between
212 the small and large domains of the β subunit on the back of the pseudo allosteric site
213 (designated as the “back cleft”) of the other heterotetramer (**Fig. 2D**). In particular, residues
214 10-14 (AKYGG) of the γ subunit make a number of hydrogen-bonding interactions with
215 several residues of the back cleft of the β subunit, which form a major part of the
216 heterotetramer-heterotetramer interface (**Fig. 2E**). Specifically, the main-chain carbonyl of
217 Pro8^G forms a hydrogen bond with the side chain of Lys165^B; the side chain of Tyr12^G forms
218 a hydrogen bond with the side chain of Asp169^B and additionally a π - π stacking interaction
219 with the side chain of Phe166^B; the main-chain amine and carbonyl of Gly13^G form a
220 hydrogen bond each with the main-chain carbonyl of Ala264^B and the side chain of His301^B,
221 respectively; the main-chain amine of Gly14^G forms a hydrogen bond with the main-chain
222 carbonyl of Glu265^B. In addition to the N-terminal region, the α_2 helix of the γ subunit also
223 makes interactions with the α_4 and α_5 helices of the β subunit, which form a minor part of
224 the heterotetramer-heterotetramer interface. In this region, the main-chain carbonyl and side
225 chain of Arg70^G on the α_2^G helix form a hydrogen bond each with the side chain of Lys165^B
226 and the main-chain carbonyl of Leu205^B, respectively. Sequence alignments showed that
227 although the N-terminal region of the γ subunit is different from that of the α and β subunits,
228 residues 10-14 (AKYGG) are strictly conserved in other mammalian NAD-IDHs and highly
229 conserved in the regulatory subunit IDH1 of yeast NAD-IDH (Liu et al., 2018; Sun et al.,
230 2019), suggesting that the N-terminal region of the regulatory subunit in other eukaryotic
231 NAD-IDHs might play a similar role in the assembly of the holoenzyme.

Figure 2.



232

233 **Figure 2. Interactions at the heterodimer-heterodimer and the heterotetramer-heterotetramer**
 234 **interfaces.**

235 (A) The $\alpha_2\beta\gamma$ heterotetramer is assembled by the $\alpha\beta$ and $\alpha\gamma$ heterodimers via their clasp domains. The
 236 color coding of the α , β and γ subunits is the same as in Figure 1. The pseudo 2-fold axis along the
 237 heterodimer-heterodimer interface, and the coplane axes of the $\alpha\beta$ and $\alpha\gamma$ heterodimers are indicated.

238 (B) Structure of the heterodimer-heterodimer interface. Middle panel: interactions at the interface
 239 consist of largely hydrophobic residues (marked by blue ovals) and a few hydrophilic residues (marked
 240 by black rectangles). Upper panel: interactions between the α and β subunits at the interface. Lower
 241 panel: interactions between the α and γ subunits at the interface. (C) Hydrogen-bonding interactions

242 between the β and γ subunits (left panel) and between the two α subunits (right panel). **(D)** A surface
243 diagram showing that the N-terminal region of the γ subunit (in blue ribbon) of one heterotetramer
244 intrudes into the back cleft of the β subunit (in green surface) of the other heterotetramer. **(E)**
245 Interactions between the N-terminal of the γ subunit and the back cleft of the β subunit. The
246 hydrogen-bonding interactions are indicated with dashed lines.

247

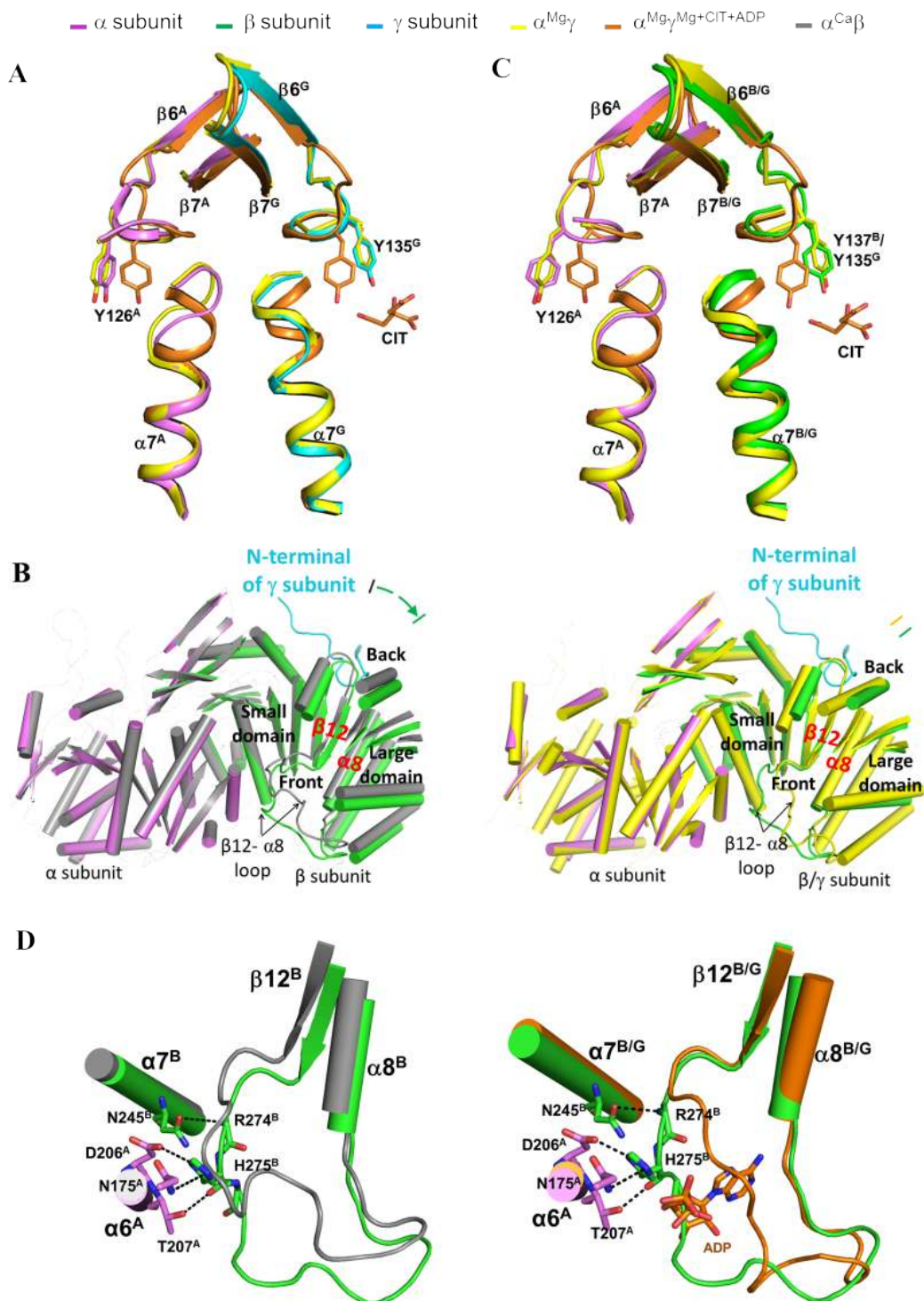
248 *The apo IDH3 holoenzyme assumes an inactive conformation*

249 Structural comparison shows that the $\alpha\gamma$ heterodimer in the apo IDH3 holoenzyme adopts an
250 inactive overall conformation similar to that in the isolated $\alpha^{\text{Mg}}\gamma$ heterodimer. Specifically, the
251 key residues at the active site (Tyr126^{A2}) and the allosteric site (Tyr135^G) assume similar
252 conformations as those in the inactive $\alpha^{\text{Mg}}\gamma$ structure rather than those in the active
253 $\alpha^{\text{Mg}}\gamma^{\text{Mg+CIT+ADP}}$ structure; the N-terminal regions of both $\alpha 7^{\text{A2}}$ and $\alpha 7^{\text{G}}$ helices at the
254 heterodimer interface assume the inactive loop conformations; and additionally, the allosteric
255 site is in proper conformation to bind the activators **(Fig. 3A)**. Intriguingly, the $\alpha\beta$
256 heterodimer in the apo IDH3 holoenzyme exhibits some conformational differences compared
257 with the isolated $\alpha^{\text{Ca}}\beta$ heterodimer. Structural analysis reveals that the insertion of the
258 N-terminus of the γ subunit into the back cleft of the β subunit pushes the large domain of the
259 β subunit to rotate away from the α subunit (the structure elements moving away from the α
260 subunit by about 1.5-3 Å) **(Fig. 3B)**. Consequently, the $\alpha\beta$ heterodimer assumes an open
261 overall conformation similar to that of the $\alpha^{\text{Mg}}\gamma$ structure rather than the compact
262 conformation of the isolated $\alpha^{\text{Ca}}\beta$ structure. In particular, the key residues at the active site
263 (Tyr126^{A1}) and the pseudo allosteric site (Tyr137^B) assume inactive conformations similar to
264 those in the $\alpha^{\text{Mg}}\gamma$ structure **(Fig. 3C)**. In addition, the N-terminal region of helix $\alpha 7^{\text{A1}}$ of the α
265 subunit at the heterodimer interface assumes a loop conformation; however, the N-terminal
266 region of helix $\alpha 7^{\text{B}}$ of the β subunit assumes a helix conformation with unknown reason.

267 At the pseudo allosteric site, the $\beta 3^{\text{B}}\text{-}\alpha 3^{\text{B}}$ loop is disordered, similar to that in the isolated
268 $\alpha^{\text{Ca}}\beta$ structure. On the other hand, the $\beta 12^{\text{B}}\text{-}\alpha 8^{\text{B}}$ loop exhibits some conformational difference
269 from that in the isolated $\alpha^{\text{Ca}}\beta$ structure **(Fig. 3D)**. Nevertheless, the N-terminal region of the
270 $\beta 12^{\text{B}}\text{-}\alpha 8^{\text{B}}$ loop maintains interactions with the $\alpha 6^{\text{A1}}$ and $\alpha 7^{\text{B}}$ helices at the heterodimer
271 interface and still occupies the ADP-binding site in the $\alpha^{\text{Mg}}\gamma^{\text{Mg+CIT+ADP}}$ structure, prohibiting
272 the ADP binding. These results together indicate that the formation of the heterooctamer
273 renders the $\alpha\beta$ heterodimer to adopt an overall conformation similar to that of the $\alpha\gamma$
274 heterodimer; however, the pseudo allosteric site remains incapable of binding the activators
275 and thus the β subunit still has no regulatory function. This explains why the $\alpha\beta$ heterodimer
276 in the holoenzyme can be allosterically activated and has normal enzymatic activity but
277 cannot bind the activators. These results also demonstrate that the structure characteristics and

278 the regulatory mechanisms of the $\alpha\beta$ and $\alpha\gamma$ heterodimers uncovered from the structure and
 279 biochemical studies of the isolated heterodimers are largely applicable to the holoenzyme.

Figure 3.



280

281 **Figure 3. Structural comparisons of the $\alpha\beta$ and $\alpha\gamma$ heterodimers in the apo holoenzyme and in**
 282 **the isolated forms.**

283 (A) Comparison of the $\alpha\gamma$ heterodimer in the holoenzyme and in the isolated forms. The color coding
 284 of the subunits and structures is shown above. The key residues at the active site (Tyr126^A) and the

285 allosteric site (Tyr135^G) assume similar conformations as those in the inactive $\alpha^{\text{Mg}}\gamma$ structure rather
286 than those in the active $\alpha^{\text{Mg}}\gamma^{\text{Mg+CIT+ADP}}$ structure. **(B)** Comparison of the overall conformation of the $\alpha\beta$
287 heterodimer in the holoenzyme with that of the isolated $\alpha^{\text{Ca}}\beta$ heterodimer (colored in gray, left panel)
288 and $\alpha^{\text{Mg}}\gamma$ heterodimer (colored in yellow, right panel). The $\alpha\beta$ heterodimer assumes an open overall
289 conformation similar to that of the isolated $\alpha^{\text{Mg}}\gamma$ heterodimer rather than the compact conformation of
290 the isolated $\alpha^{\text{Ca}}\beta$ heterodimer. For clarity, only the α helices and β strands are shown, and the loops are
291 omitted except the β_{12} - β_{8} loops of the β and γ subunits. The N-terminal of the γ subunit from another
292 heterotetramer is also shown. **(C)** Comparison of the $\alpha\beta$ heterodimer in the holoenzyme with the
293 isolated $\alpha^{\text{Mg}}\gamma$ heterodimer and $\alpha^{\text{Mg}}\gamma^{\text{Mg+CIT+ADP}}$ heterodimer. The key residues at the active site (Tyr126^A)
294 and the allosteric site (Tyr137^B) assume similar conformations as those in the inactive $\alpha^{\text{Mg}}\gamma$ structure
295 rather than those in the active $\alpha^{\text{Mg}}\gamma^{\text{Mg+CIT+ADP}}$ structure. **(D)** The β_{12} - β_{8} loop of the β subunit in the
296 holoenzyme exhibits some conformational differences from that in the isolated $\alpha^{\text{Ca}}\beta$ heterodimer but
297 still occupies the ADP-binding site in the $\alpha^{\text{Mg}}\gamma^{\text{Mg+CIT+ADP}}$ structure. The hydrogen-bonding interactions
298 of the β_{12} - β_{8} loop with the α_{7}^{B} and α_{6}^{A} helices are indicated with dashed lines.

299

300 ***The clasp domains of the $\alpha\beta$ and $\alpha\gamma$ heterodimers play a critical role in the assembly and***
301 ***allosteric regulation of the $\alpha_2\beta\gamma$ heterotetramer***

302 Our previous biochemical studies showed that the holoenzyme has notably higher activity
303 than the sum of the isolated $\alpha\beta$ and $\alpha\gamma$ heterodimers in both absence and presence of the
304 activators, suggesting that in the holoenzyme, both $\alpha\beta$ and $\alpha\gamma$ heterodimers are allosterically
305 activated and exert catalytic function (Ma et al., 2017b). Our biochemical and structural
306 studies of the $\alpha\gamma$ heterodimer showed that residues Arg97^G, Tyr135^G, and Arg272^G at the
307 allosteric site, and residues Lys151^G and Lys142^{A2} at the heterodimer interface play important
308 roles in the allosteric activation (Ma et al., 2017a). Structural analysis of the apo IDH3
309 holoenzyme shows that residues His131^{A1}, Gln139^{A1}, His131^{A2}, Gln139^{A2}, His142^B, Glu150^B,
310 His140^G, and Glu148^G of the clasp domains play an important role in the assembly of the
311 $\alpha_2\beta\gamma$ heterotetramer. To investigate the functional roles of these residues in the holoenzyme,
312 we prepared a series of mutant holoenzymes containing mutations of the key residues at the
313 allosteric site (γ_{R97A} , γ_{Y135A} , and γ_{R272A}), the pseudo allosteric site (β_{R99A} , β_{Y137A} , and β_{R274A} ,
314 corresponding to γ_{R97A} , γ_{Y135A} , and γ_{R272A}), the heterodimer interfaces ($\alpha_{1\text{K142A}}$, $\alpha_{2\text{K142A}}$,
315 $\alpha_{1\text{K142A}}\alpha_{2\text{K142A}}$, β_{K153A} , and γ_{K151A}), and the heterodimer-heterodimer interface ($\alpha_{1\text{Q139A}}$,
316 $\alpha_{2\text{Q139A}}$, $\alpha_{1\text{Q139A}}\alpha_{2\text{Q139A}}$, β_{E150A} , and γ_{E148A}), and measured their kinetic parameters in the
317 absence or presence of CIT and ADP to examine the effects of the mutations on the activity
318 and allosteric activation of the holoenzyme. The mutant $\alpha\beta$ and $\alpha\gamma$ heterodimers containing
319 mutations $\alpha_{1\text{H131A}}$, $\alpha_{2\text{H131A}}$, β_{H142A} , and γ_{H140A} could not be expressed for unknown reason(s)
320 and thus the mutant holoenzymes containing these mutations could not be obtained.

321 The wild-type holoenzyme exhibits a V_{\max} of 28.6 $\mu\text{mol}/\text{mg}/\text{min}$ and a $S_{0.5,\text{ICT}}$ of 3.54
322 mM in the absence of the activators and a V_{\max} of 30.6 $\mu\text{mol}/\text{mg}/\text{min}$ and a $S_{0.5,\text{ICT}}$ of 0.43 mM
323 in the presence of the activators, and displays a significant activation effect (8.2 folds)
324 (defined as the ratio of the $S_{0.5,\text{ICT}}$ in the presence and absence of the activators) (**Table 2 and**
325 **Fig. 4**). Compared to the wild-type holoenzyme, the mutant holoenzymes containing
326 mutations of the key residues at the allosteric site (γ_{R97A} , γ_{Y135A} , and γ_{R272A}) exhibit comparable
327 V_{\max} (<1.2 folds) and $S_{0.5,\text{ICT}}$ (<1.6 folds) in the absence of the activators, and display weak or
328 no activation effects (0.9-2.7 folds), indicating that the mutations at the allosteric site have
329 significant impacts on the activation of the holoenzyme (**Table 2 and Fig. 4**). On the other
330 hand, the mutant holoenzymes containing mutations of the key residues at the pseudo
331 allosteric site (β_{R99A} , β_{Y137A} , and β_{R274A}) also exhibit comparable V_{\max} (<1.3 folds) but slightly
332 decreased $S_{0.5,\text{ICT}}$ (<3.9 folds) in the absence of the activators, and display moderate activation
333 effects (3.1-4.3 folds), indicating that the mutations at the pseudo allosteric site have
334 insignificant impacts on the activation and function of the holoenzyme (**Table 2 and Fig. 4**).

335 The mutant holoenzymes containing mutations of the key residues at the heterodimer
336 interfaces ($\alpha_{1\text{K142A}}$, $\alpha_{2\text{K142A}}$, $\alpha_{1\text{K142A}}\alpha_{2\text{K142A}}$, β_{K153A} , and γ_{K151A}) exhibit significantly
337 decreased V_{\max} (3.1-15.1 folds) and a varied $S_{0.5}$ (0.4-3.2 folds) in the absence of the
338 activators, and display moderate or no activation effects (0.7-3.3 folds) (**Table 2 and Fig. 4**).
339 In particular, the mutant holoenzyme containing the γ_{K151A} mutation completely disrupts the
340 activation. These results indicate that the mutations at the heterodimer interface significantly
341 impair the communication from the allosteric site to the active sites of both α subunits and
342 thus have severe impacts on the activation and function of the holoenzyme. For the key
343 residues at the heterodimer-heterodimer interface, the mutant holoenzymes containing
344 mutations β_{E150A} and γ_{E148A} exhibit slightly decreased V_{\max} (about 2 folds) and $S_{0.5}$ (about 2.7
345 folds) in the absence of the activators, and display substantial activation effects (5.2-5.6 folds),
346 indicating that these mutations have minor impacts on the activation and function of the
347 holoenzyme (**Table 2 and Fig. 4**). Intriguingly, the mutant holoenzymes containing mutations
348 $\alpha_{1\text{Q139A}}$, $\alpha_{2\text{Q139A}}$, and $\alpha_{1\text{Q139A}}\alpha_{2\text{Q139A}}$ display slightly higher V_{\max} (about 1.2-1.6 folds) but
349 significantly decreased $S_{0.5,\text{ICT}}$ (6.8-14.8 folds) in the absence of the activators, and display
350 weak activation effects (<1.7 folds), indicating that these mutants are constitutively active
351 regardless the absence or presence of the activators (**Table 2 and Fig. 4**).

352 Taken together, the biochemical data demonstrate that the allosteric site plays a critical
353 role and the pseudo allosteric site has no regulatory role in the allosteric activation of the
354 holoenzyme; the heterodimer interfaces play a vital role in the allosteric regulation and
355 function of the holoenzyme; and the heterodimer-heterodimer interface plays an important
356 role in the assembly and allosteric regulation of the $\alpha_2\beta\gamma$ heterotetramer and the holoenzyme.

357

358 **Table 2.** Activities and kinetic parameters of the wild-type and mutant IDH3 holoenzymes.

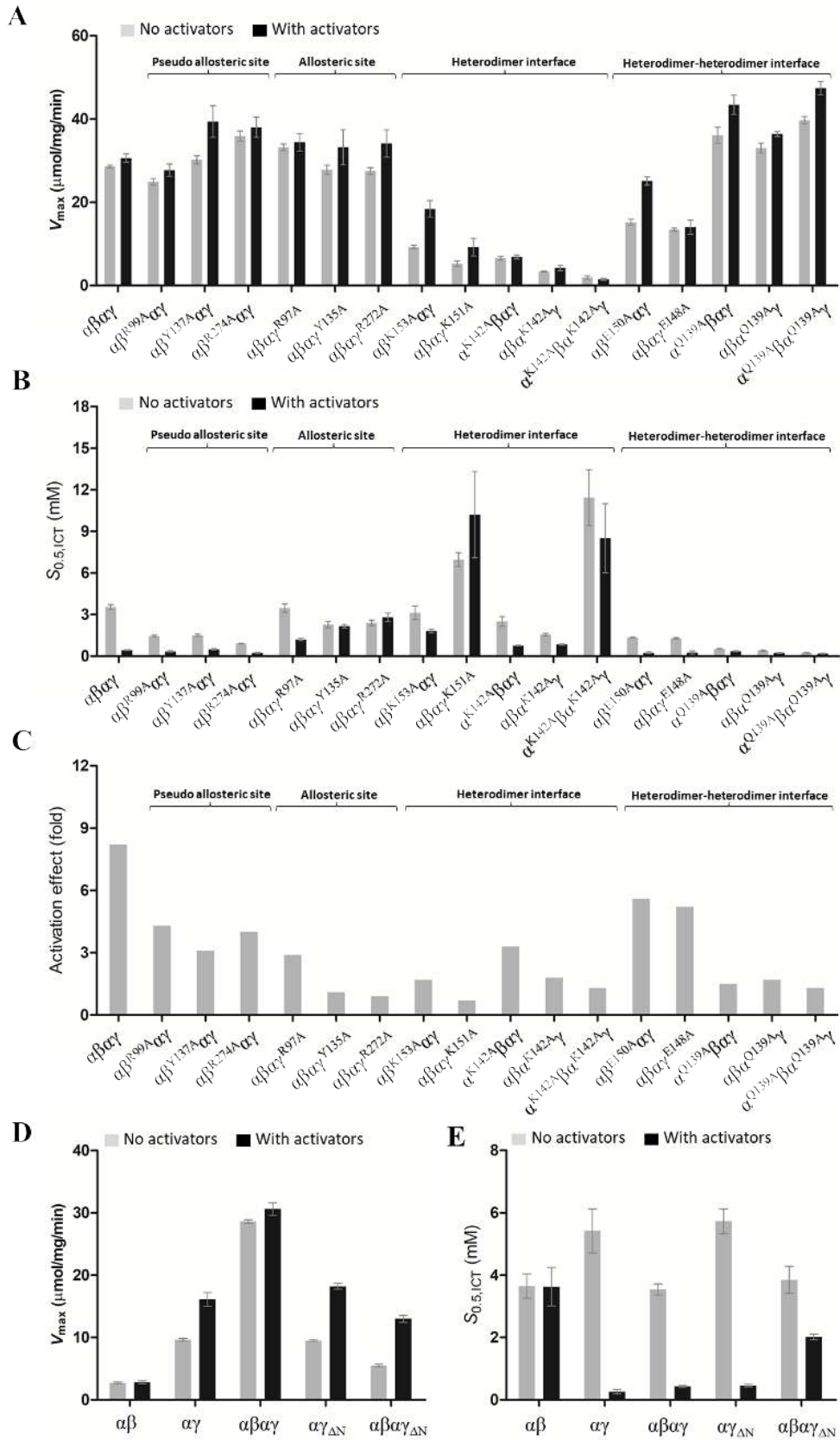
Enzyme	V_{\max} (mmol/mg/min) -activators/+activators	$S_{0.5,ICT}$ (mM) -activators/+activators	Activation effect ^a (fold)
$\alpha\beta$	2.72±0.14/2.80±0.23	3.65±0.39/3.63±0.62	1.0
$\alpha\gamma$	9.62±0.23/16.1±1.1	5.42±0.71/0.26±0.07	20.8
$\alpha\beta\alpha\gamma$	28.6±0.3/30.6±1.0	3.54±0.18/0.43±0.03	8.2
Pseudo allosteric site			
$\alpha\beta_{R99A}\alpha\gamma$	24.9±0.8/27.7±1.5	1.45±0.07/0.34±0.05	4.3
$\alpha\beta_{Y137A}\alpha\gamma$	30.2±1.0/39.4±3.8	1.50±0.09 /0.49±0.05	3.1
$\alpha\beta_{R274A}\alpha\gamma$	35.9±1.2/38.0±2.4	0.91±0.01/0.23±0.06	4.0
Allosteric site			
$\alpha\beta\alpha\gamma_{R97A}$	33.2±0.8/34.4±2.1	3.46±0.29/1.20±0.09	2.9
$\alpha\beta\alpha\gamma_{Y135A}$	27.8±1.1/33.2±4.2	2.28±0.23/2.16±0.12	1.1
$\alpha\beta\alpha\gamma_{R272A}$	27.5±0.8/34.1±3.3	2.40±0.20/2.80±0.30	0.9
Heterodimer interface			
$\alpha\beta_{K153A}\alpha\gamma$	9.21±0.43/18.4±2.0	3.13±0.49/1.80±0.13	1.7
$\alpha\beta\alpha\gamma_{K151A}$	5.24±0.63/9.19±2.12	6.96±0.50/10.2±3.1	0.7
$\alpha_{K142A}\beta\alpha\gamma$	6.53±0.44/6.84±0.45	2.50±0.35/0.76±0.03	3.3
$\alpha\beta\alpha_{K142A}\gamma$	3.33±0.11/4.20±0.61	1.55±0.10/0.84±0.04	1.8
$\alpha_{K142A}\beta\alpha_{K142A}\gamma$	1.92±0.40/1.48±0.22	11.42±2.01/8.50±2.50	1.3
Heterodimer-heterodimer interface			
$\alpha\beta_{E150A}\alpha\gamma$	15.2±0.7/25.1±1.0	1.34±0.05/0.24±0.07	5.6
$\alpha\beta\alpha\gamma_{E148A}$	13.4±0.4/14.0±1.7	1.29±0.05/0.25±0.12	5.2
$\alpha_{Q139A}\beta\alpha\gamma$	36.1±1.9/43.4±2.3	0.52±0.04/0.35±0.04	1.5
$\alpha\beta\alpha_{Q139A}\gamma$	33.0±1.2/36.4±0.6	0.40±0.05/0.23±0.03	1.7
$\alpha_{Q139A}\beta\alpha_{Q139A}\gamma$	39.7±0.9/47.4±1.6	0.24±0.03/0.18±0.03	1.3
Deletion of the N-terminal of the γ subunit (ΔN)			
$\alpha\gamma_{\Delta N}$	9.51±0.16/18.2±0.47	5.73±0.40/0.46±0.04	12.5
$\alpha\beta\alpha\gamma_{\Delta N}$	5.50±0.21/13.0±0.56	3.85±0.43/2.02±0.09	1.9

359

360 ^a Activation effect = $S_{0.5,ICT}$ (no activators) / $S_{0.5,ICT}$ (+activators).361 The enzymatic activity and kinetic data were measured at standard conditions with varied
362 concentrations of ICT in the absence or presence of the activators (CIT and ADP).

363

Figure 4.



364

365

366

Figure 4. Effects of the mutations on the activity and allosteric activation of the IDH3 holoenzyme.

367 (A) Graph presentations of the V_{\max} values, (B) the $S_{0.5,ICT}$ values, and (C) the activation effects of the
368 wild-type holoenzyme and mutant holoenzymes containing mutations of key residues at the allosteric
369 site, the pseudo allosteric site, the heterodimer interfaces, and the heterodimer-heterodimer interface in
370 the absence or presence of CIT and ADP. The activation effect is defined as the ratio of the $S_{0.5,ICT}$ in the
371 absence and presence of the activators. The detailed kinetic parameters are listed in Table 2.

372 (D) Graph presentations of the V_{\max} values and (E) the $S_{0.5,ICT}$ values of the wild-type $\alpha\beta$ and $\alpha\gamma$
373 heterodimers and holoenzyme, and the mutant $\alpha\gamma$ heterodimer and holoenzyme with the N-terminal of
374 the γ subunit removed (ΔN) in the absence and presence of CIT and ADP. The detailed kinetic
375 parameters are listed in Table 2.

376

377 *The N-terminus of the γ subunit is essential for the assembly and function of the* 378 *holoenzyme*

379 In the IDH3 holoenzyme, the N-terminal region of the γ subunit of one heterotetramer inserts
380 into the back cleft of the β subunit of the other heterotetramer to form the heterooctamer. To
381 validate the functional role of the N-terminus of the γ subunit in the assembly and function of
382 the holoenzyme, we removed the N-terminal region (residues 1-14) of the γ subunit ($\gamma_{\Delta N}$), and
383 prepared the mutant $\alpha\gamma_{\Delta N}$ heterodimer and $\alpha_2\beta\gamma_{\Delta N}$ heterotetramer. The SEC-MALS analyses
384 show that like the wild-type $\alpha\gamma$ heterodimer, the mutant $\alpha\gamma_{\Delta N}$ heterodimer exists as a dimer
385 with an average molecular weight of 84 kDa at a low concentration (2 mg/ml) and a tetramer
386 (presumably a dimer of heterodimers) with an average molecular weight of 123 kDa at a high
387 concentration (12 mg/ml) (Fig. S4A and Table S3). However, unlike the wild-type
388 holoenzyme which exists as a stable octamer at both the low and high concentrations with an
389 average molecular weight of about 284 kDa, the mutant $\alpha_2\beta\gamma_{\Delta N}$ heterotetramer exhibits an
390 average molecular weight of 106 kDa and thus appears to be a mixture of the $\alpha\beta$ and $\alpha\gamma_{\Delta N}$
391 heterodimers and the $\alpha_2\beta\gamma_{\Delta N}$ heterotetramer at the low concentration, and an average
392 molecular weight of about 125 kDa and thus appears to be a heterotetramer at the high
393 concentration (Fig. S4B and Table S3). These results indicate that deletion of the N-terminus
394 of the γ subunit does not affect the formation of the $\alpha\gamma$ heterodimer, but disrupts the formation
395 of the heterooctamer, which are in agreement with the structural data showing that the
396 N-terminus of the γ subunit is not involved in the formation of the $\alpha\gamma$ heterodimer but is
397 critical in the formation of the heterooctamer. The biochemical data also suggest that the $\alpha_2\beta\gamma$
398 heterotetramer appears to be unstable at low concentrations, and the formation of the
399 heterooctamer stabilizes the formation of the $\alpha_2\beta\gamma$ heterotetramer.

400 Consistently, the enzymatic activity assays show that the mutant $\alpha\gamma_{\Delta N}$ heterodimer
401 exhibits similar enzymatic properties as the wild-type $\alpha\gamma$ heterodimer with comparable V_{\max} ,
402 $S_{0.5}$, and activation effect (Fig. 4D and Table 2). However, compared to the wild-type

403 holoenzyme, the mutant $\alpha_2\beta\gamma_{\Delta N}$ holoenzyme exhibits a significantly low activity in both
404 absence and presence of the activators and displays a very weak activation effect (1.9 folds)
405 (**Fig. 4D and Table 2**). Specifically, the mutant $\alpha_2\beta\gamma_{\Delta N}$ holoenzyme exhibits a V_{\max} of 5.50
406 $\mu\text{mol}/\text{mg}/\text{min}$ and a $S_{0.5}$ of 3.85 mM in the absence of the activators, and a V_{\max} of 13.0
407 $\mu\text{mol}/\text{mg}/\text{min}$ and a $S_{0.5}$ of 2.02 mM in the presence of the activators, which appear to be the
408 averages of those of the $\alpha\beta$ and $\alpha\gamma$ heterodimers. This could be explained as follows: at the
409 enzymatic assay conditions, the mutant $\alpha_2\beta\gamma_{\Delta N}$ heterotetramer has a very low concentration
410 and thus exists mainly as a mixture of the $\alpha\beta$ and $\alpha\gamma_{\Delta N}$ heterodimers. Taken together, our
411 biochemical data demonstrate that the N-terminal of the γ subunit plays an important role in
412 the assembly and function of the holoenzyme.

413

414 **Discussion**

415 Human NAD-IDH or IDH3 is a key enzyme in the TCA cycle, which catalyzes the
416 decarboxylation of isocitrate into α -ketoglutarate. It exists and functions as a heterooctamer
417 composed of the $\alpha\beta$ and $\alpha\gamma$ heterodimers, and is regulated allosterically and/or competitively
418 by a number of metabolites including CIT, ADP, ATP, and NADH. Our previous biochemical
419 studies of the $\alpha\beta$ and $\alpha\gamma$ heterodimers and the holoenzyme of human IDH3 showed that in the
420 IDH3 holoenzyme, the α subunits of both $\alpha\beta$ and $\alpha\gamma$ heterodimers have catalytic function; but
421 only the γ subunit plays a regulatory role, while the β subunit plays solely a structural role
422 (Ma et al., 2017b). Our detailed structural and biochemical studies of the isolated $\alpha\gamma$ and $\alpha\beta$
423 heterodimers revealed the underlying molecular mechanisms (Liu et al., 2018; Ma et al.,
424 2017a; Sun et al., 2020; Sun et al., 2019). Specifically, the $\alpha\gamma$ heterodimer contains an
425 allosteric site in the γ subunit which can bind both CIT and ADP. The binding of CIT and
426 ADP induces conformational changes at the allosteric site, which are transmitted to the active
427 site via the heterodimer interface. This series of conformational changes renders the active
428 site to assume an active conformation favorable for ICT binding, leading to the decrease of
429 $S_{0.5,ICT}$ and hence the activation of the enzyme. In contrast, the $\alpha\beta$ heterodimer contains a
430 pseudo allosteric site in the β subunit which is structurally different from the allosteric site
431 and hence cannot bind the activators.

432 To investigate the molecular mechanism for the assembly and allosteric regulation of the
433 IDH3 holoenzyme, in this work, we determined the crystal structure of human IDH3
434 holoenzyme in apo form. In the holoenzyme, the $\alpha\beta$ and $\alpha\gamma$ heterodimers form the $\alpha_2\beta\gamma$
435 heterotetramer via their clasp domains, and two $\alpha_2\beta\gamma$ heterotetramers assemble the $(\alpha_2\beta\gamma)_2$
436 heterooctamer through the insertion of the N-terminus of the γ subunit of one heterotetramer
437 into the back cleft of the β subunit of the other heterotetramer. The holoenzyme has a

438 distorted tetrahedron architecture instead of an architecture with a pseudo 222 symmetry.
439 Specifically, the two β and two γ subunits are arranged alternately to form the inner core, and
440 the four α subunits are positioned on the periphery. The functional roles of the key residues at
441 the allosteric site, the pseudo allosteric site, the heterodimer interface, and the
442 heterodimer-heterodimer interface, as well as the N-terminus of the γ subunit in the assembly
443 and allosteric regulation of the holoenzyme are validated by mutagenesis and kinetic data.
444 The biochemical and structural data also demonstrate that the $\alpha_2\beta\gamma$ heterotetramer is unstable
445 because the heterodimer-heterodimer interface is not very tight and involves mainly
446 hydrophobic interactions. On the other hand, the $(\alpha_2\beta\gamma)_2$ heterooctamer is very stable as the
447 two $\alpha_2\beta\gamma$ heterotetramers interact with each other via two large interfaces to form a ring-like
448 architecture, and the interfaces involve both hydrophilic and hydrophobic interactions. The
449 formation of the $(\alpha_2\beta\gamma)_2$ heterooctamer stabilizes the formation of the $\alpha_2\beta\gamma$ heterotetramer in
450 the holoenzyme. These findings reveal the molecular mechanism for the assembly of the
451 heterotetramer and heterooctamer of human IDH3.

452 Structural comparison shows that in the holoenzyme, the $\alpha\gamma$ heterodimer assumes very
453 similar overall conformation as the isolated $\alpha^{\text{Mg}}\gamma$ heterodimer, and the allosteric site assumes
454 a proper conformation to bind the activators. However, the $\alpha\beta$ heterodimer exhibits some
455 conformational changes from the isolated $\alpha^{\text{Ca}}\beta$ heterodimer. The formation of the $(\alpha_2\beta\gamma)_2$
456 heterooctamer renders the $\alpha\beta$ heterodimer to adopt an overall conformation similar to that of
457 the $\alpha^{\text{Mg}}\gamma$ heterodimer rather than the compact conformation of the $\alpha^{\text{Ca}}\beta$ heterodimer.
458 Nevertheless, the pseudo allosteric site is still unable to bind the activators. Hence, the α
459 subunit of the $\alpha\beta$ heterodimer in the holoenzyme can be allosterically activated and has
460 normal catalytic function but the β subunit still has no regulatory function. These results also
461 demonstrate that the structure characteristics and the regulatory mechanisms of the $\alpha\beta$ and $\alpha\gamma$
462 heterodimers uncovered from the structure and biochemical studies of the isolated $\alpha\beta$ and $\alpha\gamma$
463 heterodimers are largely applicable to the holoenzyme.

464 Our biochemical and structural data show that the IDH3 holoenzyme exists as a stable
465 heterooctamer in both solution and structure, and functions as a heterooctamer as well. The
466 wild-type holoenzyme exhibits a notably higher activity than the sum of the activities of the
467 $\alpha\beta$ and $\alpha\gamma$ heterodimers in both the absence and presence of activators, and that the mutant
468 holoenzyme containing the α_{Y126A} mutation at the active site in either the $\alpha\beta$ or $\alpha\gamma$
469 heterodimer exhibits about 50% of the activity of the wild-type holoenzyme and displays a
470 significant activation effect; however, the mutant holoenzyme containing the α_{Y126A} mutation
471 in both $\alpha\beta$ and $\alpha\gamma$ heterodimers completely abolishes the activity (Ma et al., 2017b). These
472 results indicate that in the holoenzyme, both $\alpha\beta$ or $\alpha\gamma$ heterodimer have catalytic function and

473 can be activated by the activators, and the binding of the activators to the allosteric site in the
474 γ subunit can allosterically regulate the α subunit in both heterodimers. The structure of the
475 IDH3 holoenzyme shows that the allosteric site in the γ subunit could bind the activators but
476 the pseudo allosteric site in the β subunit remains incapable of binding the activators, and that
477 the overall conformation and the active-site conformation in both $\alpha\beta$ and $\alpha\gamma$ heterodimers are
478 suitable for allosteric activation and catalytic function. Consistently, the biochemical data
479 show that the mutations at the allosteric site have significant impacts on the activation and
480 function of the holoenzyme, whereas the mutations at the pseudo allosteric site have
481 insignificant impacts on the activation and function of the holoenzyme, indicating that the
482 allosteric site plays a critical role and the pseudo allosteric site has no regulatory role in the
483 allosteric activation of the holoenzyme. In addition, the mutations at the heterodimer
484 interfaces have severe impacts on the activation and function of the holoenzyme, indicating
485 that the heterodimer interfaces play a vital role in the communication from the allosteric site
486 to the active sites of both α subunits. Furthermore, while the β_{E150A} and γ_{E148A} mutations at the
487 heterodimer-heterodimer interface have minor impacts on the activation and function of the
488 holoenzyme; the α_{Q139A} mutation in either or both the $\alpha\beta$ and $\alpha\gamma$ heterodimers renders the
489 mutant holoenzyme constitutively active in both the absence and presence of the activators,
490 indicating that the heterodimer-heterodimer interface plays an important role in the assembly
491 and allosteric regulation of the $\alpha_2\beta\gamma$ heterotetramer and the holoenzyme. Taken together, the
492 structural and biochemical data suggest that upon the binding of the activators to the allosteric
493 site, the activation signal is transmitted from the allosteric site to the α subunits of both $\alpha\beta$
494 and $\alpha\gamma$ heterodimers through the heterodimer and heterodimer-heterodimer interfaces, leading
495 to the activation of both heterodimers in the $\alpha_2\beta\gamma$ heterotetramer and the holoenzyme. These
496 findings reveal the molecular mechanism for the allosteric regulation of the IDH3
497 holoenzyme.

498 All eukaryotes contain NAD-IDHs to carry out the catalytic function in the TCA cycle.
499 However, the composition of NAD-IDHs differs from low eukaryotes to high eukaryotes. In
500 low eukaryotes such as *Saccharomyces cerevisiae* and most single cell eukaryotes, the
501 NAD-IDH is composed of two types of subunits (IDH1 and IDH2) in 1:1 ratio. IDH1 and
502 IDH2 form the IDH1/IDH2 heterodimer which assembles the heterotetramer and further the
503 heterooctamer. In high eukaryotes such as mammals, the NAD-IDH is composed of three
504 types of subunits (α , β and γ) in 2:1:1 ratio. The α , β and γ subunits form two types of
505 heterodimers ($\alpha\beta$ and $\alpha\gamma$) which assemble the $\alpha_2\beta\gamma$ heterotetramer and further the $(\alpha_2\beta\gamma)_2$
506 heterooctamer. In either cases, the NAD-IDHs always exist and function as the heterooctamer.

507 Previous biochemical and structural studies showed that in yeast NAD-IDH, IDH2 is the
508 catalytic subunit which contains the active site, and IDH1 is the regulatory subunit which

509 contains the allosteric site (Cupp and McAlisterhenn, 1993; Lin and McAlister-Henn, 2002,
510 2003). The heterooctamer of yeast NAD-IDH exhibits an asymmetric architecture, in which
511 the regulatory IDH1 subunits form the inner core and the catalytic IDH2 subunits are
512 positioned on the outside surface, and thus the four IDH1 subunits are in two different
513 structural environments with different conformations (Taylor et al., 2008).

514 Although early biochemical studies of mammalian NAD-IDHs showed that the α subunit
515 is the catalytic subunit and the β and γ subunits are the regulatory subunits, our biochemical
516 and structural studies of human NAD-IDH or IDH3 clearly demonstrated that the α subunits
517 of both $\alpha\beta$ and $\alpha\gamma$ heterodimers have the catalytic function, the γ subunit plays the regulatory
518 role, whereas the β subunit plays no regulatory role albeit it is required for the function of the
519 holoenzyme (Ma et al., 2017b; Sun et al., 2019). Interestingly, the heterooctamer of human
520 NAD-IDH also exhibits an asymmetric architecture, in which the two β subunits and two γ
521 subunits are arranged alternately to form the inner core and the four α subunits are positioned
522 on the outer surface, and the two β subunits are in different structural environments with
523 different conformations from the two γ subunits. Structural comparison shows that the
524 heterooctamers of yeast and human NAD-IDHs exhibit almost identical architecture and
525 could be superimposed very well. These results suggest that like human NAD-IDH, only two
526 of the four IDH1 subunits in yeast NAD-IDH have allosteric regulatory function and the other
527 two have no regulatory function. This explains the biochemical data that there are only two
528 AMP-binding sites in yeast NAD-IDH holoenzyme, and provides the support evidence for the
529 speculation that the binding of AMP to all four IDH1 subunits is an artifact of excess AMP in
530 the crystallization solution (Cupp and McAlisterhenn, 1993; Lin and McAlister-Henn, 2002,
531 2003; McAlister-Henn, 2012; Taylor et al., 2008; Zhao and McAlister-Henn, 1997). These
532 findings also suggest that all eukaryotic NAD-IDHs would assume a similar asymmetric
533 architecture and employ a similar allosteric regulation mechanism.

534

535 **Materials and methods**

536 **Cloning, expression and purification**

537 The $\alpha\beta$ and $\alpha\gamma$ heterodimers and the holoenzyme of human IDH3 were prepared as described
538 previously (Ma et al., 2017b). Briefly, the DNA fragments encoding the α , β and γ subunits of
539 human IDH3 were cloned into the co-expression vector pQlinkN with the C-terminals of the β
540 and γ subunits attached with a TEV protease cleavage site and a His₆ tag to construct the
541 pQlinkN- α - β -tev-His₆ and pQlinkN- α - γ -tev-His₆ plasmids. The plasmids were transformed
542 into *E. coli* BL21 (DE3) Codon-Plus strain (Novagen). When the culture of the transformed
543 cells reached an OD₆₀₀ of 0.5, the protein expression was induced by 0.4 mM IPTG for 20 hrs
544 at 24 °C. The bacterial cells were harvested and then sonicated on ice in the lysis buffer (50
545 mM HEPES, pH 7.4, 200 mM NaCl, 0.2 mM MnCl₂, 10% glycerol, and 7.2 mM β -ME)
546 supplemented with 1 mM PMSF. The target proteins were purified by affinity
547 chromatography using a Ni-NTA column (Qiagen) with the lysis buffer supplemented with 20
548 mM and 200 mM imidazole serving as the washing buffer and elution buffer, respectively.
549 The elution fraction was dialyzed overnight against the lysis buffer supplemented with TEV
550 protease to cleave the His₆-tag of the target protein. The cleavage mixture was reloaded on a
551 Ni-NTA column and washed with the lysis buffer supplemented with 10 mM imidazole. The
552 flow-through fraction containing the target protein was further purified by gel filtration using
553 a Superdex 200 10/60 GL column (GE Healthcare) equilibrated with the storage buffer (10
554 mM HEPES, pH 7.4, 200 mM NaCl, and 5 mM β -ME). The holoenzyme was prepared by
555 co-purifying the separately expressed $\alpha\beta$ and $\alpha\gamma$ heterodimers using the same methods as for
556 the $\alpha\beta$ and $\alpha\gamma$ heterodimers. Purity of the proteins was analyzed by 12% SDS-PAGE with
557 Coomassie blue staining. Mutants of the $\alpha\beta$ and $\alpha\gamma$ heterodimers and the holoenzyme
558 containing point mutations were constructed using the QuikChange® Site-Directed
559 Mutagenesis kit (Stratagene). Expression and purification of the mutants were carried out
560 using the same methods as for the wild-type proteins.

561

562 **SEC-MALS analysis**

563 The purity, molecular mass, and size distribution of the proteins were analyzed by an
564 analytical light scattering instrument (SEC-MALS) consisting of an Agilent 1260 Infinity
565 Isocratic Liquid Chromatography System, a Wyatt Dawn Heleos II Multi-Angle Light
566 Scattering Detector, and a Wyatt Optilab T-rEX Refractive Index Detector (Wyatt
567 Technology). Analytical size exclusion chromatography was performed at 24 °C using a
568 Superdex 200 10/300 GL column (GE Healthcare) equilibrated with a mobile phase
569 containing 10 mM HEPES (pH 7.4), 200 mM NaCl, and 5 mM β -ME. 100 μ l protein solution
570 was injected into the column and eluted at a flow rate of 0.4 ml/min. The column effluent was

571 monitored simultaneously with three detectors for UV absorption, light scattering and
572 refractive index. The data were analyzed using the ASTRA software (Wyatt Technology) to
573 determine the molecular mass of the protein (Folta-Stogniew, 2006).

574

575 **Crystallization, diffraction data collection and structure determination**

576 Crystallization was performed using the hanging drop vapor diffusion method at 20 °C by
577 mixing equal volume of protein solution (10 mg/ml) and reservoir solution. Crystals of the
578 IDH3 holoenzyme grew in drops containing the reservoir solution of 0.05 M NH₄Cl, 0.05
579 Bis-Tris (pH 6.5), and 30% pentaerythritol ethoxylate. Crystals were cryoprotected using the
580 reservoir solution supplemented with 25% ethylene glycol. Diffraction data were collected at
581 100 K at BL17U1 of Shanghai Synchrotron Radiation Facility and processed with HKL3000
582 (Otwinowski Z., 1997). Statistics of the diffraction data are summarized in **Table 1**.

583 The structure of the IDH3 holoenzyme was solved with the molecular replacement
584 method implemented in program Phaser (McCoy et al., 2007) using the structures of the $\alpha\gamma$
585 heterodimer (PDB code 6KDE) and the $\alpha\beta$ heterodimer (PDB code 5GRH) as the search
586 models. Structure refinement was carried out with program Phenix and REFMAC5 (Adams et
587 al., 2010; Murshudov et al., 1997). Model building was performed with program Coot
588 (Emsley and Cowtan, 2004). Stereochemistry and quality of the structure model were
589 analyzed using programs in the CCP4 suite (Winn et al., 2011). Structure figures were
590 prepared using PyMol (Schrodinger, 2010). Statistics of the structure refinement and the final
591 structure model are also summarized in **Table 1**.

592

593 **Enzymatic activity assay**

594 The enzymatic activities of the wild-type and mutant $\alpha\beta$ and $\alpha\gamma$ heterodimers and
595 holoenzymes of human IDH3 were determined using the method as described previously (Ma
596 et al., 2017b). The standard reaction solution (1 ml) consisted of 2 ng/ml enzyme, 33 mM
597 Tris-acetate (pH 7.4), 40 mM ICT, 2 mM Mn²⁺, and 3.2 mM NAD. The activity is defined as
598 the moles of NADH produced per min per milligram of enzyme (mol/min/mg). The kinetic
599 data in the absence of the activators (CIT and ADP) were measured with varied
600 concentrations of ICT (0-40 mM), Mn²⁺ (0-10 mM), or NAD (0-10 mM) to obtain the V_{max}
601 and S_{0.5} for ICT, Mn²⁺, or NAD, respectively. The kinetic data in the presence of the activators
602 were measured at the same conditions supplemented with 1 mM CIT and 1 mM ADP. The
603 kinetic parameters were obtained by fitting the kinetic data into the non-Michaelis-Menten
604 equation “ $V=V_{max}*[S]^h/(S_{0.5}^h+[S]^h)$ ” using program Graphpad Prism (Graphpad
605 Software). All experiments were performed twice and the values were the averages of the
606 measurements with the standard errors.

607 **Protein Data Bank accession code**

608 The crystal structure of human IDH3 holoenzyme has been deposited in the Protein Data
609 Bank with accession code 7CE3.

610

611 **Conflict of interest statement**

612 The authors declare no conflict of interests.

613

614 **Acknowledgements**

615 We thank the staff members at BL17U1 of Shanghai Synchrotron Radiation Facility (SSRF)
616 and the Large-scale Protein Preparation System at the National Facility for Protein Science in
617 Shanghai (NFPS), Zhangjiang Lab, China for providing technical support and assistance in
618 data collection and analysis, and other members of our group for valuable discussion. This
619 work was supported by grants from the National Natural Science Foundation of China
620 (31870723 and 31530013) and the CAS Facility-based Open Research Program.

621

622 **Authorship contributions**

623 PS carried out the biochemical and structural studies, and participated in the data analyses.

624 TM participated in the initial biochemical and structural studies. JD conceived the study,
625 participated in the experimental design and data analyses, and wrote the manuscript.

626

627 **References**

- 628 Adams, P.D., Afonine, P.V., Bunkoczi, G., Chen, V.B., Davis, I.W., Echols, N., Headd, J.J.,
629 Hung, L.W., Kapral, G.J., Grosse-Kunstleve, R.W., McCoy, A.J., Moriarty, N.W., Oeffner,
630 R., Read, R.J., Richardson, D.C., Richardson, J. S., Terwilliger, T. C., Zwart, P. H. (2010).
631 PHENIX: a comprehensive Python-based system for macromolecular structure solution.
632 *Acta Crystallogr. D Biol. Crystallogr.* *66*, 213-221. DOI:
633 <https://doi.org/10.1107/S0907444909052925>
- 634 Al-Khallaf, H. (2017). Isocitrate dehydrogenases in physiology and cancer: biochemical and
635 molecular insight. *Cell Biosci.* *7*, 37. DOI: <https://doi.org/10.1186/s13578-017-0165-3>
- 636 Cohen, P.F., and Colman, R.F. (1972). Diphosphopyridine nucleotide dependent isocitrate
637 dehydrogenase from pig heart. Characterization of the active substrate and modes of
638 regulation. *Biochemistry* *11*, 1501-1508. DOI: <https://doi.org/10.1021/bi00758a027>
- 639 Cupp, J.R., and Mcalisterhenn, L. (1993). Kinetic-analysis of NAD⁺-isocitrate dehydrogenase
640 with altered isocitrate binding-sites-contribution of Idh1 and Idh2 subunits to regulation
641 and catalysis. *Biochemistry* *32*, 9323-9328. DOI: <https://doi.org/10.1021/bi00087a010>
- 642 Dang, L., White, D.W., Gross, S., Bennett, B.D., Bittinger, M.A., Driggers, E.M., Fantin, V.R.,
643 Jang, H.G., Jin, S., Keenan, M.C., Marks, K. M., Prins, R. M., Ward, P. S., Yen, K. E., Liao,
644 L. M., Rabinowitz, J. D., Cantley, L. C., Thompson, C. B., Heiden, M. G. V., Su, S. M.
645 (2009). Cancer-associated IDH1 mutations produce 2-hydroxyglutarate. *Nature* *462*,
646 739-U752. DOI: <https://doi.org/10.1038/nature08617>
- 647 Ehrlich, R.S., and Colman, R. (1983). Separation, recombination, and characterization of
648 dissimilar subunits of the DPN-dependent isocitrate dehydrogenase from pig heart. *J. Biol.*
649 *Chem.* *258*, 7079-7086.
- 650 Ehrlich, R.S., and Colman, R.F. (1981). Binding of ligands to half of subunits of
651 NAD-dependent isocitrate dehydrogenase from pig-heart-binding of manganous ion,
652 isocitrate, ADP and NAD. *J. Biol. Chem.* *256*, 1276-1282.
- 653 Ehrlich, R.S., Hayman, S., Ramachandran, N., and Colman, R. (1981). Re-evaluation of
654 molecular weight of pig heart NAD-specific isocitrate dehydrogenase. *J. Biol. Chem.* *256*,
655 10560-10564.
- 656 Emsley, P., and Cowtan, K. (2004). Coot: model-building tools for molecular graphics. *Acta*
657 *Crystallogr. D Biol. Crystallogr.* *60*, 2126-2132. DOI:
658 <https://doi.org/10.1107/S0907444904019158>
- 659 Folta-Stogniew, E. (2006). Oligomeric states of proteins determined by size-exclusion
660 chromatography coupled with light scattering, absorbance, and refractive index detectors.
661 *Methods Mol. Biol.* *328*, 97-112. DOI: <https://doi.org/10.1385/1-59745-026-X:97>
- 662 Gabriel, J., and Plaut, G. (1984a). Citrate activation of NAD-specific isocitrate dehydrogenase
663 from bovine heart. *J. Biol. Chem.* *259*, 1622-1628.
- 664 Gabriel, J.L., Milner, R., and Plaut, G.W. (1985). Inhibition and activation of bovine heart
665 NAD-specific isocitrate dehydrogenase by ATP. *Arch. Biochem. Biophys.* *240*, 128-134.
666 DOI: [https://doi.org/10.1016/0003-9861\(85\)90015-3](https://doi.org/10.1016/0003-9861(85)90015-3)
- 667 Gabriel, J.L., and Plaut, G.W. (1984b). Inhibition of bovine heart NAD-specific isocitrate
668 dehydrogenase by reduced pyridine nucleotides: modulation of inhibition by ADP, NAD⁺,
669 Ca²⁺, citrate, and isocitrate. *Biochemistry* *23*, 2773-2778. DOI:
670 <https://doi.org/10.1021/bi00307a037>
- 671 Hartong, D.T., Dange, M., McGee, T.L., Berson, E.L., Dryja, T.P., and Colman, R.F. (2008).
672 Insights from retinitis pigmentosa into the roles of isocitrate dehydrogenases in the Krebs
673 cycle. *Nat Genet.* *40*, 1230-1234. DOI: <https://doi.org/10.1038/ng.223>
- 674 Hurley, J.H., Dean, A.M., Koshland, D.E., Jr., and Stroud, R.M. (1991). Catalytic mechanism
675 of NADP⁺-dependent isocitrate dehydrogenase: implications from the structures of
676 magnesium-isocitrate and NADP⁺ complexes. *Biochemistry* *30*, 8671-8678. DOI:
677 <https://doi.org/10.1021/bi00099a026>
- 678 Jo, S.H., Son, M.K., Koh, H.J., Lee, S.M., Song, I.H., Kim, Y.O., Lee, Y.S., Jeong, K.S., Kim,
679 W.B., Park, J.W., Song, B. J., Huh, T. L. (2001). Control of mitochondrial redox balance
680 and cellular defense against oxidative damage by mitochondrial NADP⁺-dependent

681 isocitrate dehydrogenase. *J. Biol. Chem.* 276, 16168-16176. DOI:
682 <https://doi.org/10.1074/jbc.M010120200>

683 Kiefmann, M., Tank, S., Keller, P., Bornchen, C., Rinnenthal, J.L., Tritt, M.O.,
684 Schulte-Uentrop, L., Olotu, C., Goetz, A.E., and Kiefmann, R. (2017). IDH3 mediates
685 apoptosis of alveolar epithelial cells type 2 due to mitochondrial Ca^{2+} uptake during
686 hypocapnia. *Cell Death Dis.* 8, e3005. DOI: <https://doi.org/10.1038/cddis.2017.403>

687 Kim, S.Y., and Park, J.W. (2003). Cellular defense against singlet oxygen-induced oxidative
688 damage by cytosolic NADP^+ -dependent isocitrate dehydrogenase. *Free Radic. Res.* 37,
689 309-316. DOI: <https://doi.org/10.1080/1071576021000050429>

690 Koh, H.J., Lee, S.M., Son, B.G., Lee, S.H., Ryoo, Z.Y., Chang, K.T., Park, J.W., Park, D.C.,
691 Song, B.J., Veech, R.L., Song, H., Huh, T. L. (2004). Cytosolic NADP^+ -dependent
692 isocitrate dehydrogenase plays a key role in lipid metabolism. *J. Biol. Chem.* 279,
693 39968-39974. DOI: <https://doi.org/10.1074/jbc.M402260200>

694 Lee, S.M., Koh, H.J., Park, D.C., Song, B.J., Huh, T.L., and Park, J.W. (2002). Cytosolic
695 NADP^+ -dependent isocitrate dehydrogenase status modulates oxidative damage to cells.
696 *Free Radic. Biol. Med.* 32, 1185-1196. DOI:
697 [https://doi.org/10.1016/s0891-5849\(02\)00815-8](https://doi.org/10.1016/s0891-5849(02)00815-8)

698 Lin, A.P., Demeler, B., Minard, K.I., Anderson, S.L., Schirf, V., Galaleldeen, A., and
699 McAlister-Henn, L. (2011). Construction and analyses of tetrameric forms of yeast
700 NAD^+ -specific isocitrate dehydrogenase. *Biochemistry* 50, 230-239. DOI:
701 <https://doi.org/10.1021/bi101401h>

702 Lin, A.P., and McAlister-Henn, L. (2002). Isocitrate binding at two functionally distinct sites
703 in yeast NAD^+ -specific isocitrate dehydrogenase. *J. Biol. Chem.* 277, 22475-22483. DOI:
704 <https://doi.org/10.1074/jbc.M202534200>

705 Lin, A.P., and McAlister-Henn, L. (2003). Homologous binding sites in yeast isocitrate
706 dehydrogenase for cofactor (NAD^+) and allosteric activator (AMP). *J. Biol. Chem.* 278,
707 12864-12872. DOI: <https://doi.org/10.1074/jbc.M300154200>

708 Liu, Y., Hu, L., Ma, T., Yang, J., and Ding, J. (2018). Insights into the inhibitory mechanisms
709 of NADH on the $\alpha\gamma$ heterodimer of human NAD -dependent isocitrate dehydrogenase. *Sci.*
710 *Rep.* 8, 3146. DOI: <https://doi.org/10.1038/s41598-018-21584-7>

711 Ma, T., Peng, Y., Huang, W., and Ding, J. (2017a). Molecular mechanism of the allosteric
712 regulation of the $\alpha\gamma$ heterodimer of human NAD -dependent isocitrate dehydrogenase. *Sci.*
713 *Rep.* 7, 40921. DOI: <https://doi.org/10.1038/srep40921>

714 Ma, T., Peng, Y., Huang, W., Liu, Y., and Ding, J. (2017b). The β and γ subunits play distinct
715 functional roles in the $\alpha_2\beta\gamma$ heterotetramer of human NAD -dependent isocitrate
716 dehydrogenase. *Sci. Rep.* 7, 41882. DOI: <https://doi.org/10.1038/srep41882>

717 May, J.L., Kouri, F.M., Hurley, L.A., Liu, J., Tommasini-Ghelfi, S., Ji, Y.R., Gao, P., Calvert,
718 A.E., Lee, A., Chandel, N.S., Davuluri, R. V., Horbinski, C. M., Locasale, J. W., Stegh, A.
719 H. (2019). IDH3 α regulates one-carbon metabolism in glioblastoma. *Sci. Adv.* 5. DOI:
720 <https://doi.org/10.1126/sciadv.aat0456>

721 McAlister-Henn, L. (2012). Ligand binding and structural changes associated with allostery in
722 yeast NAD^+ -specific isocitrate dehydrogenase. *Arch. Biochem. Biophys.* 519, 112-117.
723 DOI: <https://doi.org/10.1016/j.abb.2011.10.003>

724 McCoy, A.J., Grosse-Kunstleve, R.W., Adams, P.D., Winn, M.D., Storoni, L.C., and Read, R.J.
725 (2007). Phaser crystallographic software. *J. Appl. Crystallogr.* 40, 658-674. DOI:
726 <https://doi.org/10.1107/S0021889807021206>

727 Murshudov, G.N., Vagin, A.A., and Dodson, E.J. (1997). Refinement of macromolecular
728 structures by the maximum-likelihood method. *Acta Crystallogr. D Biol. Crystallogr.* 53,
729 240-255. DOI: <https://doi.org/10.1107/S0907444996012255>

730 Nichols, B.J., Hall, L., Perry, A.C., and Denton, R.M. (1993). Molecular cloning and deduced
731 amino acid sequences of the γ subunits of rat and monkey NAD^+ -isocitrate dehydrogenases.
732 *Biochem. J.* 295, 347-350.

733 Nichols, B.J., Perry, A.C., Hall, L., and Denton, R.M. (1995). Molecular cloning and deduced
734 amino acid sequences of the α and β subunits of mammalian NAD^+ -isocitrate

735 dehydrogenase. *Biochem. J.* *310*, 917-922.

736 Otwinowski Z., M.W. (1997). Processing of X-ray diffraction data collected in oscillation
737 mode. *Methods in Enzymol.* *276*, 307-326.

738 Pavlova, N.N., and Thompson, C.B. (2016). The emerging hallmarks of cancer metabolism.
739 *Cell Metab.* *23*, 27-47. DOI: <https://doi.org/10.1016/j.cmet.2015.12.006>

740 Schrodinger, LLC (2010). The PyMOL molecular graphics system, Version 1.3r1.

741 Sun, P., Bai, T., Ma, T., and Ding, J. (2020). Molecular mechanism of the dual regulatory roles
742 of ATP on the $\alpha\gamma$ heterodimer of human NAD-dependent isocitrate dehydrogenase. *Sci.*
743 *Rep.* *10*, 6225-6225. DOI: <https://doi.org/10.1038/s41598-020-63425-6>

744 Sun, P., Ma, T., Zhang, T., Zhu, H., Zhang, J., Liu, Y., and Ding, J. (2019). Molecular basis for
745 the function of the $\alpha\beta$ heterodimer of human NAD-dependent isocitrate dehydrogenase. *J.*
746 *Biol. Chem.* *294*, 16214-16227. DOI: <https://doi.org/10.1074/jbc.RA119.010099>

747 Taylor, A.B., Hu, G., Hart, P.J., and McAlister-Henn, L. (2008). Allosteric motions in
748 structures of yeast NAD⁺-specific isocitrate dehydrogenase. *J. Biol. Chem.* *283*,
749 10872-10880. DOI: <https://doi.org/10.1074/jbc.M708719200>

750 Waitkus, M.S., Diplas, B.H., and Yan, H. (2016). Isocitrate dehydrogenase mutations in
751 gliomas. *Neuro Oncol.* *18*, 16-26. DOI: <https://doi.org/10.1093/neuonc/nov136>

752 Winn, M.D., Ballard, C.C., Cowtan, K.D., Dodson, E.J., Emsley, P., Evans, P.R., Keegan,
753 R.M., Krissinel, E.B., Leslie, A.G., McCoy, A., McNicholas, S. J., Murshudov, G. N.,
754 Pannu, N. S., Potterton, E. A., Powell, H. R., Read, R. J., Vagin, A., Wilson, K. S. (2011).
755 Overview of the CCP4 suite and current developments. *Acta Crystallogr. D Biol.*
756 *Crystallogr.* *67*, 235-242. DOI: <https://doi.org/10.1107/S0907444910045749>

757 Xu, X., Zhao, J., Xu, Z., Peng, B., Huang, Q., Arnold, E., and Ding, J. (2004). Structures of
758 human cytosolic NADP-dependent isocitrate dehydrogenase reveal a novel self-regulatory
759 mechanism of activity. *J. Biol. Chem.* *279*, 33946-33957. DOI:
760 <https://doi.org/10.1074/jbc.M404298200>

761 Yan, H., Parsons, D.W., Jin, G., McLendon, R., Rasheed, B.A., Yuan, W., Kos, I.,
762 Batinic-Haberle, I., Jones, S., Riggins, G.J., Friedman, H., Friedman, A., Reardon, D.,
763 Herndon, J., Kinzler, K. W., Velculescu, V. E., Vogelstein, B., Bigner, D. D. (2009). IDH1
764 and IDH2 mutations in gliomas. *N. Engl. J. Med.* *360*, 765-773. DOI:
765 <https://doi.org/10.1056/NEJMoa0808710>

766 Yang, B., Zhong, C., Peng, Y., Lai, Z., and Ding, J. (2010). Molecular mechanisms of "off-on
767 switch" of activities of human IDH1 by tumor-associated mutation R132H. *Cell Res.* *20*,
768 1188-1200. DOI: <https://doi.org/10.1038/cr.2010.145>

769 Yoshimi, N., Futamura, T., Bergen, S.E., Iwayama, Y., Ishima, T., Sellgren, C., Ekman, C.J.,
770 Jakobsson, J., Palsson, E., Kakumoto, K., Ohgi, Y., Yoshikawa, T., Lande 'n, M.,
771 Hashimoto, K. (2016). Cerebrospinal fluid metabolomics identifies a key role of isocitrate
772 dehydrogenase in bipolar disorder: evidence in support of mitochondrial dysfunction
773 hypothesis. *Mol. Psychiatry* *21*, 1504-1510. DOI: <https://doi.org/10.1038/mp.2015.217>

774 Zhang, D.X., Wang, Y.B., Shi, Z.M., Liu, J.Y., Sun, P., Hou, X.D., Zhang, J., Zhao, S.M.,
775 Zhou, B.H.P., and Mi, J. (2015). Metabolic reprogramming of cancer-associated fibroblasts
776 by IDH3 α downregulation. *Cell Rep.* *10*, 1335-1348. DOI:
777 <https://doi.org/10.1016/j.celrep.2015.02.006>

778 Zhao, W.N., and McAlister-Henn, L. (1997). Affinity purification and kinetic analysis of
779 mutant forms of yeast NAD⁺-specific isocitrate dehydrogenase. *J. Biol. Chem.* *272*,
780 21811-21817.

781 Zheng, J., and Jia, Z. (2010). Structure of the bifunctional isocitrate dehydrogenase
782 kinase/phosphatase. *Nature* *465*, 961-965. DOI: <https://doi.org/10.1038/nature09088>

783 Zheng, J., Yates, S.P., and Jia, Z. (2012). Structural and mechanistic insights into the
784 bifunctional enzyme isocitrate dehydrogenase kinase/phosphatase AceK. *Philos. Trans. R*
785 *Soc. Lond. B Biol. Sci.* *367*, 2656-2668. DOI: <https://doi.org/10.1098/rstb.2011.0426>

786